DOI: 10.1021/ma101003u

Macromolecules
ARTICLE

Solution-Electrospun Isotactic Polypropylene Fibers: Processing and Microstructure Development during Stepwise Annealing

Chi Wang,* Tsai-Chuan Hsieh, and Yong-Wen Cheng

Department of Chemical Engineering, National Cheng Kung University, Tainan 701, Taiwan

Received May 6, 2010; Revised Manuscript Received September 12, 2010

ABSTRACT: Isotactic polypropylene (iPP) fibers with diameters between 0.3 and 1.2 μm were successfully produced from high-temperature electrospinning solutions using a jacket-type heat exchanger to maintain the solution temperature, an infrared emitter to control the environmental temperature, and a laser heating device to heat locally the needle spinneret to a desired temperature (100−120 °C). The iPP/*o*-dichlorobenzene solutions with concentrations lower than the entanglement concentration were feasibly electrospun to produce bead-free iPP fibers, suggesting that fast solvent evaporation takes place to assist the formation of sufficiently strong chain networks prior to the jet whipping process to resist the breakup of electrified jets. Through Fourier transform infrared spectroscopy, wide-angle X-ray diffraction, small-angle X-ray scattering, and differential scanning calorimeter (DSC) analyses, the internal structure of as-spun fibers was characterized, and the annealing effect on the structure evolution was investigated. For comparison, stepwise annealing of the melt-quenched film was also carried out. For the as-spun fibers, a major mesophase with minor α-form crystal modification was found. During stepwise annealing to high temperatures, the amorphous phase remained unchanged, and the mesophase gradually transformed into stable α-form crystals prior to crystal melting. DSC results showed that both the reorganization temperature and meso → α transformation temperature in the fibers were higher than those in the melt-quenched film. On the basis of our results, a plausible mechanism for the meso → α transformation in the electrospun fibers is proposed: the initial helix reorganization takes place at the interfacial region of the mesomorphic domains, where noncrystalline chains with a preferred orientation are developed due to the elongation flow during electrospinning. After forming stable α-form nuclei, the progressive transformation of meso → α crystals toward the core of mesomorphic domain is expected.

1. Introduction

Spectacular advances in electrospinning over the past decade have resulted in the revolutionary production of numerous nanofibers from different polymers, all of which have applications in various fields.[1−6] With its tailored properties (e.g., conductivity, viscosity, and surface tension) from selected solvents, solution electrospinning is considered to outperform melt electrospinning, which is limited by the low conductivity and high viscosity of the polymer melts. During solution electrospinning, the electric field between electrodes generated by the applied voltage alters the liquid meniscus of a pendant drop suspending at the needle to become a "Taylor cone", and an electrified jet issuing from the cone apex is observed. The straight jet becomes thinner until its surface charge density is too high to sustain, leading finally to the jet whipping instability (bending instability). During the jet whipping process, severe jet stretching resulting from the mutual electric repulsive force takes place together with simultaneous solvent evaporation, yielding the dried and thin fibers deposited on the grounded collector. To date, most electrospun fibers are produced from the solution state at ambient temperature. The progress of high-temperature solution electrospinning is rather slow, and only several articles have addressed the temperature effects.[7,8] Solution electrospinning at elevated temperatures is inevitably required for some polymers, such as polyethylene (PE) and isotactic polypropylene (iPP), both of which are difficult to dissolve in common solvents at room temperature. Both PE and iPP are classified as commodity plastics with the fast expansion in production and practical application in the world. Using high-temperature solution processes, electrospun PE fibers have been reported.[9,10] Although iPP fibers can be obtained from melt electrospinning processes, the fiber diameters recovered are relatively large.[11−13] Through a sophisticated combination of three different solvents, syndiotactic PP fibers can be obtained from the solution process at room temperature.[14] Success in electrospinning iPP solution, however, has yet to be reported.

Depending on the crystallization condition, iPP chains can develop three crystal modifications (α, β, and γ).[15,16] Among them, the monoclinic α-form is the most stable modification. Using specific nucleating agents, the metastable β-form, with a trigonal symmetry, can be obtained. The γ-form is orthorhombic and normally appears in the low molecular weight PP species or under high-pressure crystallization. Within these three crystal modifications, iPP chains take a 3_1 helical structure with either right-handed (RH) or left-handed (LH) characters. According to the orientation of the methyl group, which can orient either upward or downward with respect to the main chain, four different helical conformations are found in the crystal modification. In addition to the above three modifications, iPP can also develop a unique structure called the mesomorphic phase (mesophase) under particularly rapid quenching from the melt state.[17] The mesophase of the iPP is controversial, and there have been some debates regarding its origin. Nata and Corradini[18] considered the mesophase as an intermediate state between the amorphous and crystalline phase. Grebowicz et al.[19] proposed its

*Corresponding author: Tel +886-6-2757575 ext 62645; Fax +886-6-2344496; e-mail chiwang@mail.ncku.edu.tw.

 Published on Web 10/07/2010

formation as conformationally disordered crystals, the so-called "condis crystals". Some researchers suggested the iPP mesophase to be a paracrystalline structure or nanocrystallites having α- or β-form crystals.[20−22] However, on the basis of theoretical calculations of the scattering patterns, Corradini et al.[23] concluded that the mesophase is distinct from the α- or β-formed crystals. Recent findings confirmed that the mesophase contains clusters of ordered helical chain segments with a random assembly of helical handedness.[24,25] This is in contrast to stable α-form crystals, which possess the regular bilayer packing of RH and LH helices in the crystal. By transmission electron microscopy (TEM), clusters with diameters of ∼10 nm were observed to fill the entire mesomorphic sample.[25] Moreover, atomic force microscopy (AFM) revealed that the diameter of mesomorphic domains increased with annealing time at a given annealing temperature.[26] Cooling rate is the key factor that determines the formation of mesophase; fast cooling of iPP melts yields the mesophase, whereas a low cooling rate gives rise to the α-form crystals.[17] As characterized by wide-angle X-ray diffraction (WAXD) (Cu target), the 2θ measurements of 15.0° and 21.6° are the signatures of the mesophase; the former is associated with the interchain distance, and the latter is due to the 3_1 helical chains.[24]

In this paper, the preparation of electrospun iPP fibers is realized by a high-temperature solution process, which mainly consists of a heating oil jacket for maintaining solution temperature and a laser heating device to control the needle temperature for electrospinning. Solution concentration effects on the fiber morphologies are investigated. The internal structure of as-spun fibers exhibits a major fraction of mesophase together with traces of stable α crystalline forms. Using several analytical tools, the microstructure development of electrospun fibers during stepwise annealing is also studied, and the results are compared with those obtained from melt-quenched iPP film. Our results provide valuable information and answer a crucial question: How does the mesophase developed from the electrospun iPP fibers transform into the stable monoclinic form (α-form) during annealing? On the basis of our results, a plausible mechanism is proposed.

2. Experimental Section

Electrospinning of iPP Solution. Taiwan Propylene Co. supplied the iPP powder without additives. The melt index of the powder was 3.0 g/10 min, and its viscosity-average molecular weight (M_w) was 2.8×10^5 g/mol. *o*-Dichlorobenzene (*o*-DCB) was used as a solvent to prepare the iPP solution for electrospinning. To enhance the solution conductivity, a predetermined amount of tetra-*n*-butylammonium perchlorate (Bu_4NClO_4) soluble salt was added to the iPP/*o*-DCB solution.

To prepare solutions with different wt % concentrations, weighed amounts of iPP and *o*-DCB were mixed for 2 h at 130 °C. The salt concentration was relative to the mass of the solution. Figure 1 shows the schematic setup of the high-temperature electrospinning system. A homemade jacket-type heat exchanger was used to maintain the polymer solution at a desirable electrospinning temperature. This was fulfilled through the circulation of heated silicone oil by a pumping system connected to an oil bath, where the temperature could be adjusted up to 150 °C.[8] Because of the long and thin needle used, a significant temperature gradient was found along the needle spinneret, causing an apparent temperature difference for solutions within the jacket tube and at the needle end. This temperature drop led to gel formation at the surface of the Taylor cone adjacent to the needle end, leading to cone distortion and an uncontrolled electrospinning process. To resolve the gel formation problem, high-energy laser light was used to shine locally on the needle spinneret. This noncontacting heating device was found to maintain the needle temperature effectively at a temperature as high as 120 °C, well above the gel and crystallization temperature of the present iPP solutions. By manipulating the laser output power and the focusing

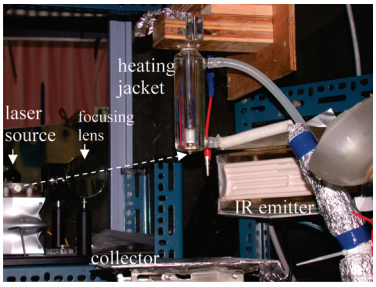

Figure 1. Schematic setup of the high-temperature electrospinning apparatus. A jacket-type heat exchanger is designed to maintain the temperature of polymer solution at a constant value by circulating heated silicone oil. An IR emitter is used to control the environmental temperature by its throughput and distance to the spinning apparatus. A laser heating device is used to locally control the temperature of needle spinneret. The needle temperature can be varied by the output power of the laser light as well as the focusing lens. The dashed line shows the path of laser light.

lens, the temperature of the solution flowing out of the needle end could be varied. In addition, the temperature of the electrospinning environment was controlled by an infrared (IR) emitter.[9] Solvent evaporation is rapid when the solution temperature approaches the boiling temperature of the solvent used (180.5 °C for *o*-DCB), resulting in gradual cone shrinkage and leading to unstable electrospinning. For our apparatus, a cone-jet electrospinning mode was maintained at a temperature of up to 100 °C. By measuring the temperature of the pendant drop at the needle end using a thermocouple, the solution working temperature for electrospinning was determined. When the system reached thermal equilibrium, the homogeneous polymer solution was electrospun into the fiber forms according to the procedure reported previously.[8]

Film samples were prepared by melting the as-received iPP powders for 10 min at 200 °C, followed by rapid quenching into liquid nitrogen. The thickness of the melt-quenched film was ∼20 μm.

Characterization of Solution and Fibers. To avoid gel formation during electrospinning, it is important to determine the lowest applicable temperature prior to the process. Calorimetric measurements were carried out using a Perkin-Elmer DSC7 at several rates of 2, 5, and 10 °C/min to cool the homogeneous iPP solutions to room temperature. The sol-to-gel temperature (T_{gel}) was determined by temperature extrapolation of the exothermic peak to a rate of 0 °C/min, with the corresponding exothermic enthalpy (ΔH_{gel}) used to evaluate the gel content. With subsequent heating at a rate of 10 °C/min, the gel-to-sol temperature ($T_{m,gel}$) was also determined from the endothermic peak. For the as-spun fibers and melt-quenched film, DSC heating at a rate of 10 °C/min was performed to observe the heat-flow until crystal melting.

The morphology and diameter of the electrospun fibers were observed using a scanning electron microscope (SEM, Hitachi S4100). AFM observations were carried out in air using a Nanoscope Multimode IIIa ((Digital Instruments) operated in Tapping Mode. Height and phase data were collected simultaneously. In-situ IR spectra of samples during stepwise annealing were obtained at 1 cm^{-1} resolution by a Perkin-Elmer Spectrum 100 spectrometer equipped with a Mettler FP900 hot stage. The temperature protocol for stepwise annealing is shown in Figure S1. WAXD and small-angle X-ray scattering (SAXS) were carried out with graphite-monochromatized Cu Kα radiation using a Bruker diffractometer (NanoSTAR Universal System). In-situ diffraction intensity profiles of samples during annealing were obtained using a vacuum-assisted heating device.

3. Results and Discussion

Precipitates of iPP and/or gels are developed when the homogeneous iPP/*o*-DCB solution at a high temperature is cooled down below the T_{gel}.[27] Our results showed that an iPP gel was

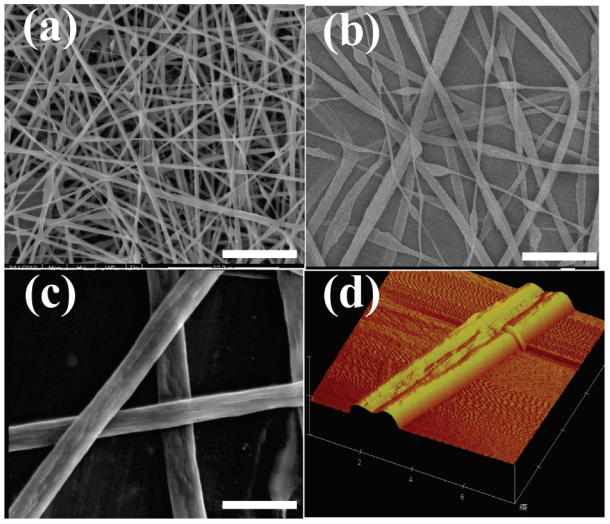

Figure 2. SEM images of electrospun fibers obtained from solutions with different iPP concentrations: (a) 1, (b) 5, and (c) 8 wt %. (d) AFM image of a ribbon-shaped fiber in (c). The scale bar is 5 μm.

likely to form from solutions with an iPP concentration higher than 5 wt %. The formation of iPP gel and precipitate at the spinneret outlet during electrospinning blocks the solution flow and interrupts the process. Thus, determining the T_{gel} of a given solution and maintaining the temperature of the spinneret above this temperature for smooth spinning are important. On the basis of the DSC results, the T_{gel} of the 8 wt % iPP solution was 80.7 °C, whereas the addition of 0.5 wt % salt to the solution led to a slight increase of T_{gel} to 82.2 °C (Figure S2). For the iPP solution with a concentration of 5 wt %, the determined T_{gel} was 70.8 °C. To ensure continuous electrospinning, the temperature of the spinneret was controlled to ~100 °C by adjusting the laser heating setup.

Fiber Morphology of the Electrospun iPP Fibers. The formation of chain networks by entanglements in the electrospinning solution is a general prerequisite to prepare bead-free fibers.[28,29] For a given M_w of polymers, the entanglement concentration (c_e) is estimated by $c_e \sim 2M_e/M_w$, where M_e is the entanglement molecular weight of the polymer in the melt state. M_e depends on the polymer type and is relatively independent of the temperature. The reported value of M_e for iPP is 6900 g/mol,[30] which produces a calculated c_e value of 5 wt % for the solution used. Previous studies have shown that c_e represents the minimum concentration to yield electrospun products exhibiting fiberlike structures. However, depending on the strength of entangled network in the solution state, solutions with concentrations of ca. 1.5−2.0 c_e are required to produce uniform polymer fibers.[28,29] In contrast, solutions with concentrations lower than c_e generally yield polymeric particulates.

Figure 2 shows the iPP fibers electrospun from solutions with different concentrations. Of particular importance is the appearance of uniform fibers at an iPP concentration of 1 wt %, which is much lower than the c_e calculated for the present iPP species. To yield fiberlike products, previous studies have shown that it is the electrified jet, not the prepared solution, which should be sufficiently concentrated to be in the entangled solution regime to prevent the Raleigh instability.[8] By controlling solvent evaporation during electrospinning, several strategies can be applied to render the unentangled solution prior to processing to become entangled. Electrospinning at elevated temperatures is one approach. Another possible approach is the addition of salts to the solution to enhance its conductivity, and this also accounts for the present findings. A shorter straight jet prior to the jet whipping process is desirable because the electrified jet experiences a higher electric field under the needle−plate electrode configuration.[8] The length reduction of the straight jet is readily fulfilled by salt addition, which leads to significant jet stretching and a high jet velocity accompanied by enhanced solvent evaporation at the jet surface. Although uniform fibers with an average diameter of 286 nm can be obtained from electrospinning the 1 wt % iPP solution, the removal of residual Bu_4NClO_4 salts is generally required for further application. Without harming the as-spun iPP fibers, a short-time immersion in the pure *o*-DCB solvent at ambient temperature is found to be very effective for salt extraction. This was confirmed by the FTIR spectra. As shown in Figure 2, ribbonlike fibers began to be produced from the electrospinning of the 5 wt % solution and became the dominant feature in that obtained from the 8 wt % solution. Using AFM and SEM, the width and thickness of the iPP ribbons obtained from the 8 wt % solution were measured to be 1.8 ± 0.2 μm and 450 ± 50 nm, respectively. Koombhongse et al.[31] attributed the ribbonlike fibers to the rapid formation of a solid skin during electrospinning because of fast solvent evaporation. The deformation of the whipping jet with this skin layer by mutual electric forces between the jet segments leads to the final appearance of ribbons.

Electrospun iPP fibers can also be obtained from the melt state through melt electrospinning.[11−13] Because of their high viscosity and low melt conductivity, as-spun iPP fibers possess diameters of several tens of micrometers. Using a viscosity-reducing additive, melt-electrospun iPP fibers with diameters of 840 nm were obtained at a spinning temperature of 270−320 °C.[13] The long-term exposure of iPP melts to such high temperatures may lead to thermal degradation, resulting in the inferior mechanical strength of the fibers. Compared with melt electrospinning, our results indicate that solution electrospinning is a more versatile process for readily preparing iPP fibers with submicrometer diameters, provided that the solution properties and processing variables are appropriately controlled.

Crystal Structure of As-Spun iPP Fibers. WAXD intensity profiles of as-spun fibers prepared from solutions with different concentrations are shown in Figure 3a, in which the small diffraction peak at $2\theta = 8.4°$ was associated with the added salt. The salt could be completely extracted by immersing the fibers in *o*-DCB solvent at room temperature for a short time, as indicated by the WAXD curves of the fibers from the 1 and 5 wt % iPP solutions. Our additional studies showed that Bu_4NClO_4 salt crystals remained intact prior to melting at ~200 °C. The WAXD profile of ribbonlike fibers (Figure 2c) shown in Figure 3b is used to demonstrate the peak deconvolution for determining the crystal fractions. The typical diffraction peaks associated with the α-form crystals were observed at $2\theta = 14.2°$, 16.7°, 18.2°, 20.5°, and 21.2° for the planes of (110), (040), (130), (111), and (131), respectively. In addition, the diffraction peaks associated with the mesophase were clearly resolved at $2\theta = 14.8°$ and 20.9°. After the deconvolution of the intensity profile,[32] the fractions of the α-form crystal and mesophase are determined to be 0.13 and 0.34, respectively. Similar analyses were carried out for the other two fibers. For fibers electrospun from the 5 wt % iPP solution, the fractions of the α-form and mesophase are 0.09 and 0.38. On the other hand, the fractions of the α-form and mesophase are 0.03 and 0.44 for the fibers from the 1 wt % solution. Regardless of the diameter and shape of fibers, the amorphous fraction is constant (~0.53). Moreover, the mesophase is the dominant structure in the as-spun fibers, suggesting the occurrence of rapid jet cooling due to fast solvent evaporation. Fast solvent

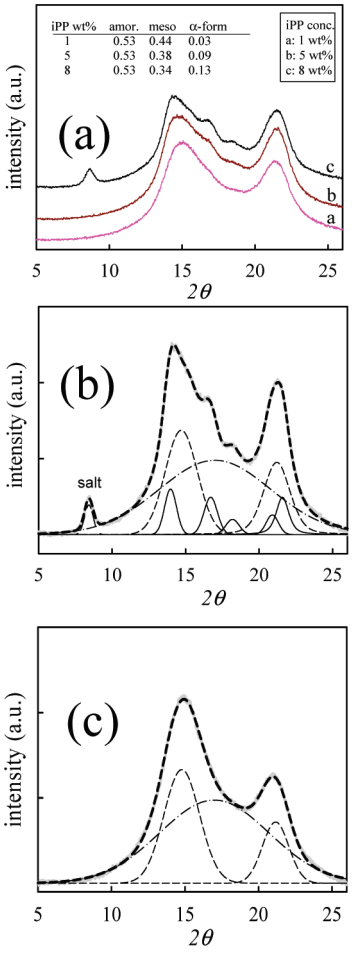

Figure 3. (a) WAXD profiles of iPP fibers electrospun from solutions with different concentrations, (b) deconvolution of intensity profile of fibers electrospun from 8 wt % iPP solution, and (c) deconvolution of intensity profile of melt-quenched film. The thick gray line is the observed intensity profile, and the thick dashed line is the summation of the intensity contributed from the mesophase (thin dashed lines), α-form crystals (thin solid lines), and amorphous phase (thin dash-dotted line).

evaporation at the jet surface yields a skin layer, which hinders the subsequent evaporation (diffusion) of residual solvent in the inner core. Driven by the electric repulsive forces between the jet segments, the deformation of the electrified jets by the solidlike skin finally leads to the ribbonlike fibers.[31] In consideration of the relative solvent evaporation rates of the skin and core of the solution jet, the mesophase and α-form crystals were expected to reside in the skin layer and core section of the ribbonlike fiber.

For the melt-quenched iPP films, only the mesophase was obtained, and no diffraction peaks relevant to the α-form crystal were seen (Figure 3c). This is consistent with the previous reports,[17] which showed that the rapid cooling of iPP melts leads to the formation of a pure mesophase. By means of intensity deconvolution, the fractions of the mesophase and amorphous phase were calculated to be 0.38 and 0.62, respectively. Thus, electrospun fibers possessed a lower amorphous fraction than the melt-quenched film. It is attributed to the flow-induced chain orientation during jet whipping in the electrospinning process.

In the following sections, ribbonlike fibers electrospun from the 8 wt % iPP solution were studied to reveal the thermal effects on the structure evolution, and the results were compared with those obtained from melt-quenched film.

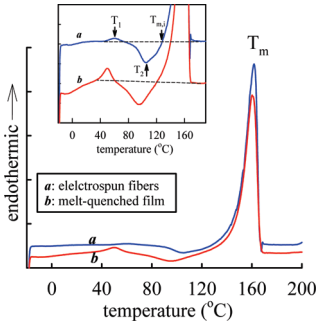

Figure 4. DSC heating traces of electrospun fibers (curve *a*) and melt-quenched film (curve *b*). The apparent melting temperature is T_m. The inset shows the magnification of the small heat-flow region, showing the presence of a small endotherm and a relatively large exotherm before the initial crystal melting at the temperature of $T_{m,i}$. The peak temperature of the enotherm and exotherm are denoted by T_1 and T_2, respectively.

The DSC heating traces of the as-spun fibers and melt-quenched films at a rate of 10 °C/min are shown in Figure 4. The enlarged portion of the small heat flow at the low-temperature transition is provided in the inset. For the as-spun fibers, a small endotherm with a peak temperature (T_1) of 61.6 °C was observed, followed immediately by a relatively large exotherm with a peak temperature (T_2) of 105.5 °C. The apparent melting temperature (T_m) was 161.8 °C, but initial crystal melting took place at the temperature ($T_{m,i}$) of 129.7 °C. The small endotherm is related to the heat gain during chain reorganization in the mesophase, and the exotherm is attributed to the transformation of the mesophase to α-form crystallites.[25,33] In other words, a small energy is required to trigger the reorganization process of helical chains from the random assembly of handedness to the correct registration with respect to its neighboring helices. Within the mesomophic domains, the "newborn" clusters with the correct molecular packing serve as the initial α-form nuclei for subsequent crystallization, possibly through a secondary nucleation theme.[25]

A similar DSC heating curve was observed for the melt-quenched films, and the corresponding values of T_1, T_2, and $T_{m,i}$ were 49.6, 97.0, and 120.7 °C, respectively. Using a melting enthalpy of 209 J/g for the 100% α-form crystals, the calculated crystallinity fraction of the fibers was 0.449, which is slightly higher than that of the melt-quenched films at 0.410. Our DSC results indicate that chain reorganization and transformation are more difficult with electrospun fibers than with melt-quenched films.

Structure Evolution in the Electrospun iPP Fibers during Annealing. During the stepwise annealing of the as-spun fibers at higher temperatures, the intensity of the mesomorphic diffractions decreased, and the monoclinic diffraction peaks intensified (Figure 5a). Similar observations were detected for the melt-quenched film samples (Figure 5b). After deconvoluting the intensity profiles, the fraction of individual phases was determined and plotted as a function of T_a, as shown in parts a and b of Figure 6 for the electrospun fibers and melt-quenched films, respectively. The temperatures of T_1, T_2, and $T_{m,i}$ obtained from DSC are indicated for reference. It is important to note that the amorphous fraction remained unchanged in both the fibers and the film samples during annealing prior to crystal melting, indicating that the amorphous phase is not involved in the reorganization and transformation processes. Similar findings were found by Konishi et al.[32] in their study of iPP crystallization from the prequenched mesophase. The fractions of α-form crystal and mesophase remained unchanged

during the chain reorganization of the mesophase at temperatures lower than T_1. At temperatures higher than T_1, however, a gradual decrease in the fraction of mesophase, along with an increase in α-form content, occurred. At the annealing temperature T_2, a significant amount of mesophase transformed into α-form crystallites. Both the electrospun fibers and melt-quenched films exhibited the same T_a dependence of reorganization and meso → α transformation behavior, except for their differences in T_1, T_2, and $T_{m,i}$. It appears that the presence of α-form crystals in the as-spun fibers does not promote meso → α transformation.

To detect the chain conformation of the samples during stepwise annealing, in-situ FTIR was performed. IR traces the conformational variation of chains in different physical states. Several regularity bands associated with the different critical lengths (m) of isotactic sequences were reported.

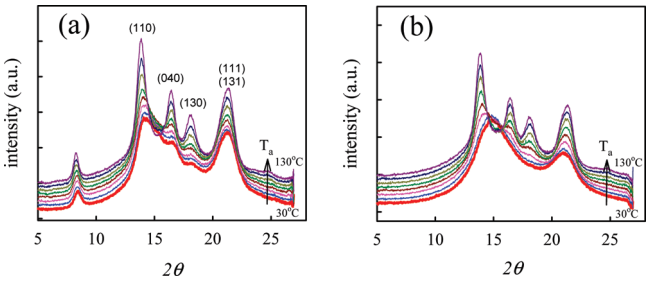

Figure 5. WAXD intensity profiles of (a) electrospun fibers and (b) melt-quenched film during stepwise annealing at different temperatures of 30, 50, 80, 90, 100, 110, 120, and 130 °C.

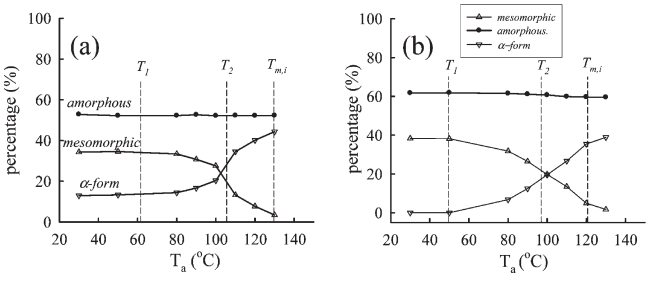

Figure 6. T_a dependence of amorphous phase, mesophase, and α-form crystal during stepwise annealing of (a) electrospun fibers and (b) melt-quenched film. T_1 and T_2 are peak temperatures for the reorganization and meso → α transformation determined from the DSC heating trace as shown in Figure 4.

The presence of bands at 973, 998, 841, and 1220 cm^{-1} is attributed to the minimum m values of 3−4, 10, 12, and 14 repeating units in the helical sequences, respectively.[34,35] The band at 1156 cm^{-1} was relevant with the nonhelical sequences (amorphous phase). It has been pointed out that 973 cm^{-1} band also has a component from chains with irregular conformations (amorphous phase).[36] Both 841 and 1220 cm^{-1} bands are associated with the crystalline region (either mesophase or α-form crystal) and are often used to characterize the iPP crystallinity. However, the absorbance of 1220 cm^{-1} is ca. 1 order of magnitude lower than that of 841 cm^{-1}. Provided that 1220 cm^{-1} band is applied for a quantitative analysis, thick sample is generally required in order to obtain reliable data due to its low absorbance. For our thin fibers, it is more appropriate to use the high absorbance of the 841 cm^{-1} band to determine the iPP crystallinity. Figure 7a shows the expanded IR spectra of electrospun iPP fibers annealed at different T_a from 30 to 170 °C. As the T_a is increased, the absorbance of bands of 841, 973, and 998 cm^{-1} continuously decrease. Band broadening and band shifting, which are associated with the increase in the number of defects and expansion of unit cell, respectively, are clearly seen. It should be noted that 1168 cm^{-1} band is also associated with the crystalline region due to its final disappearance at 170 °C. The order degree of the regularity band of 1168 cm^{-1} is higher than 841 cm^{-1} but lower than 1220 cm^{-1};[35] however, the corresponding m value is not fully determined yet (possibly ranging between 12 and 14). Because of the overlapping of the interested bands, deconvolution of the band pairs of 973/998 and 1156/1168 cm^{-1} is required to correctly determine the its individual contribution. To fulfill the attempt, the Gaussian−Lorentzian function was applied, and typical deconvolution results are shown in Figure S3. Taking into the consideration of changes in band half-widths, it is preferable to measure the band area as a function of T_a. Figure 7b shows the T_a dependence of normalized band area with respect to that obtained from 30 °C. It is evident that the area under the amorphous band remains constant prior to initial crystal melting in agreement with the WAXD results. More importantly, for the respective intensities of the isotactic sequence bands ($m \geq 10$), there is a linear decrease of band intensity with increasing temperature to about $T_{m,i}$, beyond which the absorbance decreases more rapidly. The linear reduction of band intensity is caused by the effect of absorption coefficient,[37] which is a function of temperature, whereas the rapid drop in band intensity is attributed to the crystal melting. A similar trend was observed for the melt-quenched films during

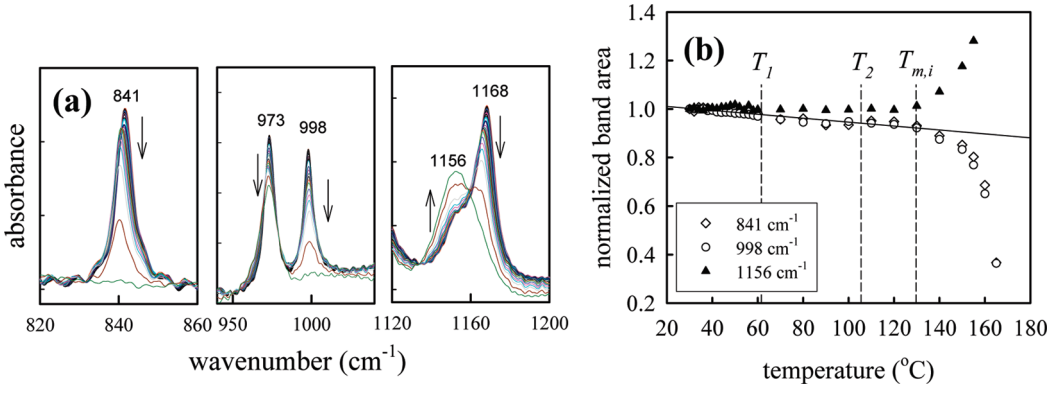

Figure 7. (a) Expanded FTIR spectra of electrospun fibers annealed stepwisely from 30 to 170 °C. The direction of thin arrow indicates the height variation of corresponding bands with increasing annealing temperature. The wavenumbers of 841, 973, 998, and 1156 cm^{-1}, which correspond to m = 12, 3−4, 10, and amorphous phase, respectively. The tick interval of the absorbance axis is 0.1. (b) Annealing temperature dependence of the normalized band area of the corresponding wavenumber. At 30 °C, the integrated band area is 1.49, 1.50, and 2.53 for the band of 1156, 841, and 998 cm^{-1}, respectively.

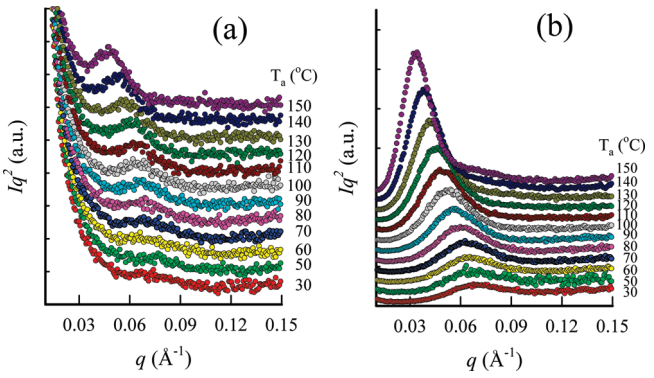

Figure 8. SAXS results of (a) electrospun fibers and (b) melt-quenched film during stepwise annealing at different temperatures, T_a. For the electrospun fibers, strong zero-angle scattering is observed, which is absent for the melt-quenched film.

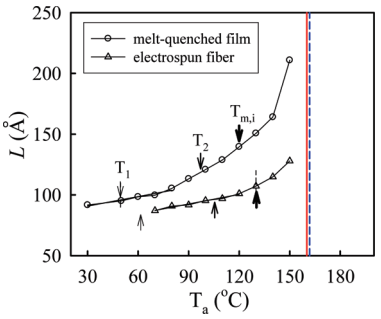

Figure 9. T_a dependence of interdomain distance for the electrospun fibers and melt-quenched film. The thin, intermediate, and thick arrows are used for the T_1, T_2, and $T_{m,i}$, respectively. The vertical solid and dashed lines are used for the T_m of the film and electrospun fibers, respectively. Note that T_m of fibers is slightly higher than that of the film.

stepwise annealing (Figure S4). Our FTIR results suggest that no significant conformational variations of iPP chains in the fibers occurred during the processes of reorganization and meso → α transformation. Since the amorphous fraction remains intact during the stepwise annealing process until $T_{m,i}$, the likeness of cold crystallization of supercooled liquid after partially "melting" of the mesomorphic domains is ruled out. In other words, solid−solid phase transition is likely to be the main mechanism to account for the processes of reorganization and meso → α transformation.

Recent studies seem to conclude that mesomorphic structures consist of chain aggregations (clusters or nodules) with ordered helical conformations along the chain direction but with disordered packing in the lateral direction.[24,25] The mesomorphic domains, which fill the entire melt-quenched sample, have an average size of 10−20 nm and are frequently seen under TEM and AFM observations.[25,33] To trace the variation of morphological features during annealing, SAXS was conducted. The Lorentz-corrected intensity plots as a function of scattering vector, q ($= 4\pi \sin\theta/\lambda$), are shown in parts a and b of Figure 8 for the fibers and film samples, respectively. For the melt-quenched films at room temperature, a discernible scattering peak at 0.0685 Å^{-1} was detected. Stepwise annealing led to a more pronounced scattering peak with the peak position (q_m) shifting toward the low q region. In contrast, two main features were observed from the SAXS results of electrospun fibers: there was an upturning of the scattering intensity at the low q region (q < 0.03 Å^{-1}), and no detectable SAXS peak was observed until 70 °C, at which point a barely seen SAXS peak was first detected. Further annealing to a higher temperature gradually caused the scattering peak to become more pronounced and to move to a lower q_m.

The strong SAXS intensity in the low q region indicates the presence of long-range disorder, which persisted until major crystal melting occurred at 160 °C. This diffuse scattering,[38] which is frequently observed in conventional wet or dry spinning processes, can be attributed to the existence of nanovoids in the electrospun fibers. On the basis of Guinier's plot (Figure S5), the radii of the nanovoids were determined to be 8.6−19.1 nm in the as-spun fibers, and they slightly decreased to 7.4−18.9 nm at the annealing temperature of 150 °C. The spectrum of the void sizes ranges similarly to that of the fibers obtained from conventional solution spinning.[38] Compared with the melt-quenched film, the absence of the SAXS peak at room temperature suggests the lowering of the scattering contrast. This implies that the density difference between the mesomorphic domain and amorphous phase is significantly reduced in the as-spun iPP fibers. The mesophase is considered an intermediate state with a density higher than that of the amorphous phase but lower than that of the crystalline phase. In the melt-quenched film, the density contrast between the mesomorphic domain and amorphous phase is sufficient for the feasibility of SAXS measurements. Significant jet stretching occurs during electrospinning, producing preferential chain orientations along the spinning line. Because of the elongational flow character of electrospinning, in the as-spun fibers the iPP chains in the amorphous phase were preferentially oriented along the fiber axis. Thus, the density of the amorphous phase slightly increased, and the contrast for SAXS was reduced, leading to the absence of the SAXS long-range ordering at room temperature (Figure 8a). Subsequent thermal annealing at 70 °C (> T_1) provided not only the ordering perfection of the mesophase but also the relaxation of the stretched chains in the amorphous phase. Both enhanced the scattering contrast for SAXS and caused the initial appearance of a small SAXS peak.

The position of the scattering peak was used to determine the interdomain distance (L) based on the Bragg law: $L = 2\pi/q_m$. The scale of L represents the distance between either mesomorphic domains formed at low T_a or lamellar domains developed at high T_a.[25,33] Figure 9 shows the T_a dependence of L. The characteristic temperatures obtained from DSC are indicated as eye guides. At a given T_a, the L in the electrospun fibers was evidently smaller than that in the melt-quenched films. The value of L increased continuously with T_a, which is consistent with previous results using a continuous heating process at a rate of 4 °C/min.[25] For melt-quenched films, three regimes are identified. During the reorganization of helices in the mesophase (30−70 °C), L slightly increases due possibly to thermal expansion. The increase of L with T_a becomes more apparent during the meso → α transformation prior to reaching the $T_{m,i}$, followed by a significant L increase during crystal melting. For electrospun fibers, the first regime is missing, and the slope of the second regime is low.

In sum, four main features are recovered from the annealing results of the as-spun and melt-quenched iPP samples. First, the mesophase transforms into α-form crystals before initial crystal melting at $T_{m,i}$. Second, the amorphous phase fraction remains constant up to the temperature $T_{m,i}$. Third, the transition temperatures (T_1, T_2, and $T_{m,i}$) for the electrospun fibers are higher than those for the melt-quenched films. Finally, the major difference between the as-spun fibers and melt-quenched films is the chain conformation in the interdomain region; the former possesses noncrystalline chains with a preferred orientation along the fiber, whereas

the latter contains chains of lower degree alignment without specific orientations.

A Plausible Mechanism for Chain Reorganization and Crystal Transformation. More conclusive evidence has been provided recently to conclude that the mesomorphic domains consist of bundles of helical chains with a 3-fold structure.[24,25,33] In spite of the regular sequence along the chain axis (as revealed by FTIR spectra), the lateral arrangement of these helices with RH and LH sequences is completely random (as indicated by WAXD patterns). In contrast, the bilayer structure of the RH and LH helices is required in stable α crystals. The mesophase is an intermediate structure between the crystalline and amorphous phases[18] and is essentially stable at ambient temperature.[39] Because of its excess free energy, however, the mesophase is in a position to transform into low-energy α crystals, provided that a sufficient thermal (not mechanical)[38] energy is supplied to overcome the energy barrier. In other words, the reorganization process is necessarily triggered by heating to an elevated temperature of T_1 to induce α-crystal nuclei with correct helical-handedness arrangements. After forming α-form nuclei, crystal transformation (or crystallization) readily takes place and spreads over the entire mesomorphic domain,[25] as indicated by a small exotherm with a peak temperature of T_2.

Two crucial questions are addressed as follows: Where is the initial location for chain reorganization to take place? How does the meso → α transformation proceed? For the first question, three possible locations are suggested: in the amorphous region, inside the mesomorphic domains, or in the interfacial region of the mesomorphic domains. The reorganization is not likely to be initiated in the amorphous region as the amorphous fraction remains unchanged prior to crystal melting (Figures 6 and 7). If the transitions were to take place within the mesomorphic domains, the transition temperatures would be approximately identical in the as-spun fibers and melt-quenched films. On the contrary, our results showed that the values of T_1 and T_2 in the fibers were ca. 10 °C higher than those in the film samples. Because of chain constraints during elongation flow, the oriented and rigid amorphous chains at the interface of mesophase in the as-spun fibers exhibited low mobility, resulting in a high-temperature requirement for chain reorganization. On the basis of our DSC results, the initial reorganization was more likely to occur at the interfacial region of the mesomorphic domains, and a small energy was required to overcome the energy barrier to trigger the process.

For the observed meso → α transformation, Androsch[33] recently proposed two possible mechanisms, specifically, the rewinding (reversal of helical hand) and chain translation mechanisms. The former involves the gradual adjustment of the helical stem conformation, whereas the latter preserves the initial helical hands during the transformation process.[40] Our FTIR results showed that there was no detectable variation in chain conformations prior to initial crystal melting (Figure 7b and Figure S4). This suggests that the molecular stems at the interface of mesomorphic domains move to the right position to form new α-form nuclei without changing their handedness. The subsequent crystallization, also called the meso → α transformation, immediately proceeds and grows toward the inner core of the mesomorphic domains, preserving the helical hands.

4. Conclusions

A unique design for high-temperature electrospinning is presented. The temperatures of the solution, spinneret, and the environment can be well-controlled by a heating jacket, laser source, and IR emitter, respectively. By adjusting the processing parameters and solution properties, semicrystalline iPP is electrospun into the nanofiber form, which is generally infeasible with conventional room-temperature processes. Solvent evaporation is expected to occur rapidly when solution electrospinning is performed at elevated temperatures, producing two unique features. The first is the increase in the polymer concentration in the electrified jet prior to jet whipping. This leads to the production of uniform fibers despite the fact that the prepared solution possessed a polymer concentration lower than the entanglement concentration. The second is the retardation of chain crystallization in the solution state, resulting in the major formation of the mesophase in the as-spun fibers. The microstructure of the electrospun fibers is characterized using DSC, FTIR, WAXD, SAXS, SEM, and AFM. Some unique features that have not been reported in the literature are obtained.

Acknowledgment. This work was supported by the National Science Council of Taiwan (NSC94-2216-E-006-004, NSC96-2918-I-006-011) and the Landmark Project of National Cheng Kung University (B0147). The helpful comments provided by the reviewer on the interpretation of FTIR results are also acknowledged.

Supporting Information Available: Temperature protocol used for stepwise annealing; DSC results for the determination of gel temperature, gel content, and melting temperature of gel; typical deconvolution of FTIR spectra of electrospun fibers; in-situ FTIR results of the melt-quenched film during annealing; Guinier plots of the SAXS data for the determination of the radius of nanovoids. This material is available free of charge via the Internet at http://pubs.acs.org.

References and Notes

(1) Huang, Z. M.; Zhang, Y. Z.; Kotaki, M.; Ramakrishna, S. *Compos. Sci. Technol*. **2003**, *63*, 2223.
(2) Li, D.; Xia, Y. *Adv. Mater*. **2004**, *16*, 1151.
(3) Ramakrishna, S.; Kazutoshi, F.; Teo, W. E.; Lim, T. C.; Ma, Z. In *An Introduction to Nanofibers*; World Scientific Co. Pte. Ltd: Singapore, 2005.
(4) Reneker, D. H.; Fong, H. *Polymeric Nanofibers*; ACS Symposium Series 918; American Chemical Society: Washington, DC, 2006.
(5) Greiner, A.; Wendorff, J. H. *Angew. Chem., Int. Ed*. **2007**, *46*, 5670.
(6) Reneker, D. H.; Yarin, A. L. *Polymer* **2008**, *49*, 2387.
(7) Desai, K.; Kit, K. *Polymer* **2008**, *49*, 4045–4050.
(8) Wang, C.; Chien, H. S.; Hsu, C. H.; Wang, Y. C.; Wang, C. T.; Lu, H. A. *Macromolecules* **2007**, *40*, 7973.
(9) Givens, S. R.; Gardner, K. H.; Rabolt, J. F.; Chase, D. B. *Macromolecules* **2007**, *40*, 608–610.
(10) Rein, D. M.; Shavit-Hadar, L.; Khalfin, R. L.; Cohen, Y.; Shuster, K.; Zussman, E. *J. Polym. Sci., Polym. Phys*. **2007**, *45*, 766–773.
(11) Larrondo, L.; Manley, St. J. R. *J. Polym. Sci., Polym. Phys*. **1981**, *19*, 909.
(12) Lyons, J.; Li, C.; Ko, F. *Polymer* **2004**, *45*, 7597–7603.
(13) Dalton, P. D.; Grafahrend, D.; Klinkhammer, K.; Klee, D.; Möller, M. *Polymer* **2007**, *48*, 6823–6833.
(14) Lee, K.-H.; Ohsawa, O.; Watanaba, K.; Kim, I.-S.; Givens, S. R.; Chase, B.; Rabolt, J. F. *Macromolecules* **2009**, *42*, 5215–5218.
(15) Lotz, B.; Wittmann, J. C.; Lovinger, A. J. *Polymer* **1996**, *27*, 4979.
(16) Bruckner, S.; Meille, S. V.; Petraccone, V.; Pirozzi, B. *Prog. Polym. Sci*. **1991**, *16*, 361.
(17) Zia, Q.; Androsh, R.; Radusch, H.-J.; Piccarolo, S. *Polymer* **2006**, *47*, 8163–8172.
(18) Nata, G.; Corradini, P. *Nuovo Cimento Suppl* **1960**, *15*, 40.
(19) Grebowicz, J.; Lau, J. F.; Wunderlich, B. *J. Polym. Sci., Polym. Symp*. **1984**, *71*, 19.
(20) Hosemann, R.; Wilke, W. *Makromol. Chem*. **1968**, *118*, 230.
(21) Murthy, N. S.; Minor, H.; Bednarczyk, C.; Krimm, S. *Macromolecules* **1993**, *26*, 1712.
(22) Ferrero, A.; Ferracini, E.; Mazzavillani, A.; Malta, V. *J. Macromol Sci., Phys*. **2000**, *B39*, 109.
(23) Corradini, P.; De Rosa, C.; Guerra, G.; Petraccone, V. *Polym. Commun*. **1989**, *30*, 281.
(24) Lotz, B. *Eur. Phys. J. E: Soft Matter Biol. Phys*. **2000**, *3*, 165.

(25) Wang, Z.-G.; Hsiao, B. S.; Srinivas, S.; Brown, G. M.; Tsou, A. H.; Cheng, S. Z. D.; Stein, R. S. *Polymer* **2001**, *42*, 7561–7566.
(26) Zia, Q.; Radusch, H.-J.; Androsch, R. *Polymer* **2007**, *48*, 3504–3511.
(27) Nakaoki, T.; Inaji, Y. *Polym. J.* **2002**, *34*, 539–543.
(28) McKee, M. G.; Wilkes, G. L.; Colby, R. H.; Long, T. E. *Macromolecules* **2004**, *37*, 1760–1767.
(29) Shenoy, S. L.; Bates, W. D.; Frisch, H. L.; Wnek, G. E. *Polymer* **2005**, *46*, 3372.
(30) Eckstein, A.; Suhm, J.; Friedrich, C.; Maier, R. D.; Sassmannshausen, J.; Bochmann, M.; Mülhaupt, R. *Macromolecules* **1998**, *31*, 1335–1340.
(31) Koombhongse, S.; Liu, W.; Reneker, D. H. *J. Polym. Sci., Polym. Phy. Ed.* **2001**, *39*, 2598–2606.
(32) Konishi, T.; Nishida, K.; Kanaya, T. *Macromolecules* **2006**, *39*, 8035–8040.
(33) Androsch, R. *Macromolecules* **2008**, *41*, 533–535.
(34) Konishi, T.; Nishida, K.; Kanaya, T.; Kaji, K. *Macromolecules* **2005**, *38*, 8749–8754.
(35) Zhu, X.; Yan, D.; Yao, H.; Zhu, P. *Macromol. Rapid Commun.* **2009**, *21*, 354–357.
(36) Brookes, A.; Dyke, J. M.; Hendra, P. J.; Meehan, S. *Specrtochim. Acta, Part A* **1997**, *53*, 2313–2321.
(37) Hanna, L. A.; Hendra, P. J.; Maddams, W.; Willis, H. A.; Zichy, V.; Cudby, M. E. A. *Polymer* **1988**, *29*, 1843–1847.
(38) Statton, W. O. *J. Polym. Sci.* **1956**, *22*, 385–397.
(39) Qiu, J.; Wang, Z.; Yang, L.; Zhao, J.; Niu, Y.; Hsiao, B. S. *Polymer* **2007**, *48*, 6934–6947.
(40) Lotz, B.; Mathieu, C.; Thierry, A.; Lovinger, A. J.; De Rosa, C.; de Ballesteros, O. R.; Auriemma, F. *Macromolecules* **1998**, *31*, 9253–9257.